Data in Brief 4 (2015) 328–331

Contents lists available at ScienceDirect

Data in Brief

journal homepage: www.elsevier.com/locate/dib

Data Article

# Lipid and protein maps defining arterial layers in atherosclerotic aorta

Marta Martin-Lorenzo [a], Benjamin Balluff [b], Aroa S. Maroto [a], Ricardo J. Carreira [b], Rene J.M. van Zeijl [b], Laura Gonzalez-Calero [a], Fernando de la Cuesta [c], Maria G Barderas [c], Luis F Lopez-Almodovar [d], Luis R Padial [e], Liam A. McDonnell [b], Fernando Vivanco [a,f], Gloria Alvarez-Llamas [a,*]

[a] Department of Immunology, IIS-Fundacion Jimenez Diaz, UAM, REDinREN, Madrid, Spain
[b] Center for Proteomics and Metabolomics, Leiden University Medical Center, Leiden, The Netherlands
[c] Department of Vascular Physiopathology, Hospital Nacional de Paraplejicos, SESCAM, Toledo, Spain
[d] Department of Cardiac Surgery, Hospital Virgen de la Salud, SESCAM, Toledo, Spain
[e] Department of Cardiology, Hospital Virgen de la Salud, SESCAM, Toledo, Spain
[f] Department of Biochemistry and Molecular Biology I, Universidad Complutense, Madrid, Spain

ARTICLE INFO

*Article history:*
Received 12 June 2015
Received in revised form
16 June 2015
Accepted 16 June 2015
Available online 24 June 2015

ABSTRACT

Subclinical atherosclerosis cannot be predicted and novel therapeutic targets are needed. The molecular anatomy of healthy and atherosclerotic tissue is pursued to identify ongoing molecular changes in atherosclerosis development. Mass Spectrometry Imaging (MSI) accounts with the unique advantage of analyzing proteins and metabolites (lipids) while preserving their original localization; thus two dimensional maps can be obtained. Main molecular alterations were investigated in a rabbit model in response to early development of atherosclerosis. Aortic arterial layers (intima and media) and calcified regions were investigated in detail by MALDI-MSI and proteins and lipids specifically defining those areas of interest were identified. These data further complement main findings previously published in

DOI of original article: http://dx.doi.org/10.1016/j.jprot.2015.06.005
* Corresponding author.
*E-mail address:* galvarez@fjd.es (G. Alvarez-Llamas).

http://dx.doi.org/10.1016/j.dib.2015.06.005

J Proteomics (M. Martin-Lorenzo et al., J. Proteomics. (In press); M. Martin-Lorenzo et al., J. Proteomics 108 (2014) 465–468.) [1,2].


Specifications table

| | |
|---|---|
| Subject area | Biology |
| More specific subject area | Cardiovascular disease, MSI development and application to arterial tissue |
| Type of data | Table and figure |
| How data was acquired | MALDI-MSI, FTICR |
| Data format | Analyzed |
| Experimental factors | Specific and careful tissue treatment was applied as previously published [1] |
| Experimental features | |
| Data source location | LUMC (Leiden, The Netherlands), IIS-Fundación Jiménez Díaz (Madrid, Spain) |
| Data accessibility | |

Value of the data

- A novel unexplored ex vivo imaging approach in cardiovascular disease;
- 30 μm high spatial resolution is applied to investigate atherosclerosis tissue layers;
- This is the first time specific protein localization and alteration in response to atherosclerosis is shown by MALDI-MSI;
- TMSB4X up-regulation in atherosclerosis is firstly identified at its original location.

## 1. Data, experimental design, materials and methods

### 1.1. Data

Specific molecular features (*m*/*z* values) were identified by MALDI-MSI, corresponding to proteins and lipids specifically defining intima, media or calcified regions in atherosclerotic rabbit aorta (Fig. 1).

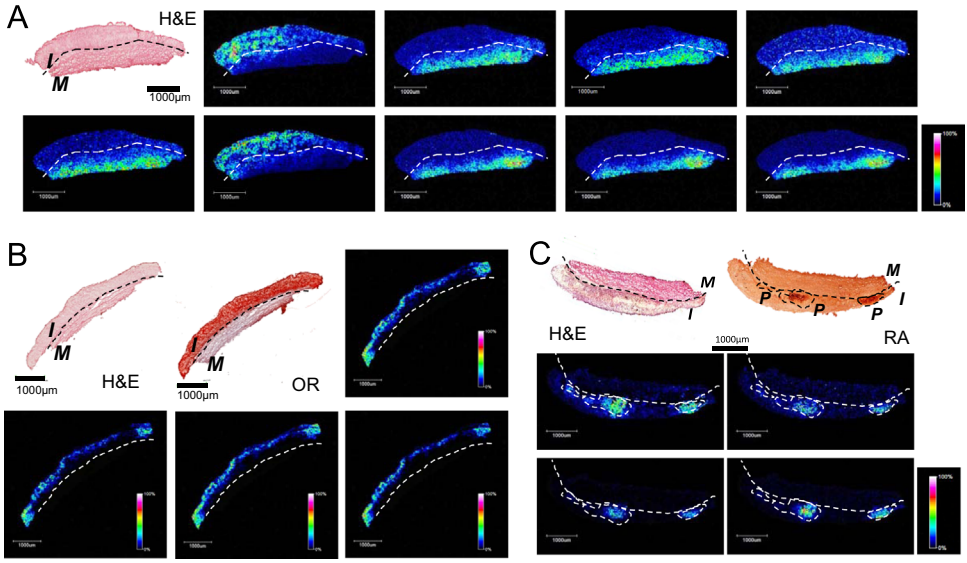


**Fig. 1.** Representative MALDI-MSI images for proteins (A) and lipids (B, C) in rabbit aorta. Intima (I) and media (M) layers and calcified regions (*P*) in the intima are defined by specific *m*/*z* values. Characterization of samples is made according to histology: H&E, Oil-Red (OR) and Red Alizarin (RA).

**Table 1**
MALDI-MSI *m/z* values with specific localization in the intima or media layer are shown (left column): $x^P$ means specifically located in the calcified region of the intima layer. Comparison between healthy and atherosclerotic tissues is also included (right column):↑increased in atherosclerosis;↓decreased in atherosclerosis; *P*: pathologic (atherosclerotic) tissue; *C*: control (healthy) tissue. Bold numbers show statistical significance ($p$ Value $< 0.05$, Mann–Whitney test). Identification was performed by FT-ICR measurements, MaTisse database, MSiMass list database and literature [12,13].

| | **Arterial localization** | | | **Atherosclerosis** | | | **Molecule** |
|---|---|---|---|---|---|---|---|
| ***m/z*** | **Media** | **Intima** | ***p*-Value** | **Trend** | **Fold change (*P*/*C*)** | ***p*-Value** | |
| **Proteins** | | | | | | | |
| **3011** | | x | **0.0108** | ↑ | 1.67 | **0.0022** | SEL1L, IQGAP1, GANAB, NCSTN, UGDH, CYBA, YWHAG, MIF, EIF2S3, SYNM, ITGA5, NDUFS7, COL12A1, VASN, EEF1A1, MYBPC1, HBA1-2, ENO1, UBA1, CA3, MUC5B |
| **3553** | x | | **0.0022** | ↓ | 0.64 | **0.0152** | NSF, PSMC4, ACTB, MYL2, PKM2, HSPD1 |
| **3569** | x | | **0.0022** | ↓ | 0.67 | **0.0303** | DHRS7, ACTB, MYL2, PKM2, ERP44, S100A6 |
| **4597** | x | | **0.0022** | ↓ | 0.92 | 0.4589 | – |
| **4614** | x | | **0.0022** | ↓ | 0.93 | 0.6494 | HBB |
| **4762** | | x | **0.0303** | ↑ | 3.00 | **0.0022** | TMSB4X |
| **4778** | | x | **0.0303** | ↑ | 2.07 | **0.0022** | – |
| **5620** | x | | **0.0022** | ↓ | 0.58 | **0.0087** | – |
| **6182** | x | | **0.0022** | ↓ | 0.49 | **0.0022** | – |
| **6199** | x | | **0.0022** | ↓ | 0.57 | **0.0152** | – |
| **Lipids** | | | | | | | |
| **255** | | x | **0.0152** | ↑ | 4.98 | **0.0022** | SFA |
| **518** | | x | **0.0022** | ↑ | 8.74 | **0.0022** | Lysolipids |
| **520** | | x | **0.0260** | ↑ | 4.58 | **0.0260** | Lysolipids |
| **522** | | x | **0.0022** | ↑ | 5.64 | **0.0022** | LPC (0:0/18:1), lysolipids |
| **535** | | $x^P$ | **0.0381** | ↑ | 4.21 | **0.0381** | – |
| **536** | | $x^P$ | 0.3524 | ↑ | 1.42 | 0.1714 | – |
| **568** | | $x^P$ | 0.1714 | ↑ | 3.57 | 0.0667 | – |
| **675** | | $x^P$ | 0.0667 | ↑ | 6.84 | **0.0190** | PA |
| **676** | | $x^P$ | 0.1143 | ↑ | 4.61 | **0.0381** | PA + PG |
| **691** | | $x^P$ | 0.0667 | ↑ | 4.43 | **0.0381** | SM + PA + PE − Cer |
| **722** | | $x^P$ | 0.1143 | ↑ | 4.76 | 0.1143 | PC + PE |
| **800** | | x | **0.0022** | ↑ | 3.74 | **0.0022** | SM |
| **864** | | x | **0.0087** | ↑ | 9.77 | **0.0022** | PG |
| **865** | | x | **0.0087** | ↑ | 6.54 | **0.0022** | PI |
| **866** | | x | **0.0260** | ↑ | 1.03 | **0.0022** | PC |
| **891** | | x | 0.0931 | ↑ | 6.52 | **0.0022** | Glc − GP + PI |
| **893** | | x | **0.0433** | ↑ | 6.18 | **0.0411** | PS |
| **895** | | $x^P$ | 0.3874 | ↑ | 1.51 | 0.1320 | TG |

*m/z* values with specific location, and fold change in response to atherosclerosis early development are compiled in Table 1. Tentative identification was performed and is also shown.

### *1.2. Experimental design*

A rabbit model of atherosclerosis was developed as previously published [3] to investigate molecular alterations in arterial tissue in response to atherosclerosis. High-spatial-resolution MALDI-MSI was applied to comparatively analyze histologically-based arterial regions of interest from control and atherosclerotic aortas.

### *1.3. Materials and methods*

The ascending aortic section of each animal was dissected, snap frozen in liquid nitrogen without any fixation and stored at −80 °C [4,5].Three different MALDI-MSI protocols were applied for the

detection of proteins [2], lipids [6] and metabolites [7,8]. Public libraries of MALDI-MSI data, MSiMass list database [9] and MaTisse [10] were used to assign identity of the most significantly altered protein molecular feature using a mass tolerance of $\pm 3$ Da [11]. Lipid molecular identification was performed by using exact mass measurements, peak peaking and spatial filtering combined with Lipidsmap database using a tolerance of $\leq 0.005$ Da, as previously published [12,13]. For comparison between control and atherosclerotic tissue, a random selection of the whole spectra sets from these regions were then imported into ClinProTools 3.0 (Bruker Daltonik) where they underwent smoothing, baseline subtraction, mass spectral alignment and normalization. Mann–Whitney non-parametric tests were performed using GraphPad Prism software.

## Acknowledgments

This work is financially supported by the Cyttron II project "Imaging Mass Spectrometry", ISCIII (PI11/01401, PI13/01873, CP09/00229) and IDCSalud (Grant number 3371/002). MML is funded by Fundación Conchita Rabago and gratefully acknowledges the travel funding supplied by SePROT and the COST Action BM1104 for the Short Term Scientific Missions to LUMC. BB and RC are funded by the Marie Curie Actions of the European Union (BB no. 331866, SITH FP7-PEOPLE-2012-IEF, RC no. 303344, ENIGMAS FP7-PEOPLE-2011-IEF).

These results are lined up with the Spanish initiative on the Human Proteome Project (SpHPP).

## References

[1] M. Martin-Lorenzo, B. Balluff, A.S. Maroto, R.J. Carreira, R.J.M. van Zeijl, L. Gonzalez-Calero, F. de la Cuesta, M.G. Barderas, L. F. Lopez-Almodovar, L.R. Padial, L.A. McDonnell, F. Vivanco, G. Alvarez-Llamas, J. Proteomics (2015). (In press).

[2] M. Martin-Lorenzo, B. Balluff, A. Sanz-Maroto, R.J. van Zeijl, F. Vivanco, G. Alvarez-Llamas, et al., J. Proteomics 108 (2014) 465–468.

[3] M. Martin-Lorenzo, I. Zubiri, A. Maroto, L. Gonzalez-Calero, M. Posada-Ayala, F. de la Cuesta, et al., KLK1 and ZG16B proteins and arginine-proline metabolism identified as novel targets to monitor atherosclerosis, acute coronary syndrome and recovery, Metabolomics (2014)http://dx.doi.org/10.1007/s11306-014-0761-8.

[4] K. Chughtai, R.M. Heeren, Mass spectrometric imaging for biomedical tissue analysis, Chem. Rev. 110 (5) (2010) 3237–3277.

[5] S. Meding, A. Walch, MALDI imaging mass spectrometry for direct tissue analysis, Methods Mol. Biol. 931 (2013) 537–546.

[6] S.M. Willems, R.A. van, Z.R. van, A.M. Deelder, L.A. McDonnell, P.C. Hogendoorn, Imaging mass spectrometry of myxoid sarcomas identifies proteins and lipids specific to tumour type and grade, and reveals biochemical intratumour heterogeneity, J. Pathol. 222 (4) (2010) 400–409.

[7] E.A. Jones, R. Shyti, R.J. van Zeijl, S.H. van Heiningen, M.D. Ferrari, A.M. Deelder, et al., Imaging mass spectrometry to visualize biomolecule distributions in mouse brain tissue following hemispheric cortical spreading depression, J Proteomics 75 (16) (2012) 5027–5035.

[8] T.J. Dekker, E.A. Jones, W.E. Corver, R.J. van Zeijl, A.M. Deelder, R.A. Tollenaar, et al., Towards imaging metabolic pathways in tissues, Anal. Bioanal. Chem. (2014).

[9] L.A. McDonnell, A. Walch, M. Stoeckli, G.L. Corthals, MSiMass list: a public database of identifications for protein MALDI-MS imaging, J. Proteome Res. (2013).

[10] S.K. Maier, H. Hahne, A.M. Gholami, B. Balluff, S. Meding, C. Schoene, et al., Comprehensive identification of proteins from MALDI imaging, Mol. Cell Proteomics 12 (10) (2013) 2901–2910.

[11] B. Balluff, S. Rauser, S. Meding, M. Elsner, C. Schone, A. Feuchtinger, et al., MALDI imaging identifies prognostic seven-protein signature of novel tissue markers in intestinal-type gastric cancer, Am. J. Pathol. 179 (6) (2011) 2720–2729.

[12] K. Chughtai, L. Jiang, T.R. Greenwood, K. Glunde, R.M. Heeren, Mass spectrometry images acylcarnitines, phosphatidylcholines, and sphingomyelin in MDA-MB-231 breast tumor models, J. Lipid Res. 54 (2) (2013) 333–344.

[13] J. Schiller, O. Zschornig, M. Petkovic, M. Muller, J. Arnhold, K. Arnold, Lipid analysis of human HDL and LDL by MALDI-TOF mass spectrometry and (31)P NMR, J. Lipid Res. 42 (9) (2001) 1501–1508.